mTrack: Enabling Long-Term Mouse Social Behavior Analysis through RFID-Vision Hybrid Tracking

Xingyuming Liu
School of Computer Science
Peking Univerisity
Beijing, China
liuxym@pku.edu.cn

Bo Liang
School of Computer Science
Peking University
Beijing, China
rambo@pku.edu.cn

Haobo Wang
School of Computer Science
Peking University
Beijing, China
haobowang25@stu.pku.edu.cn

Zhonghao Li
National Institute on Drug Dependence
Peking University
Beijing, China
lzhongh@hsc.pku.edu.cn

Qirui Liu
School of Computer Science
Peking University
Beijing, China
qirui_liu@pku.edu.cn

Yan-Xue Xue
National Institute on Drug Dependence
Peking University
Beijing, China
yanxuexue@bjmu.edu.cn

Yunhuai Liu
School of Computer Science
Peking University
Beijing, China
yunhuai.liu@pku.edu.cn

Chenren Xu*†
School of Computer Science
Peking University
Beijing, China
chenren@pku.edu.cn

Abstract

Tracking-based social behavior analysis of lab animals, especially mice, is crucial for research in biology, medicine, and psychology. However, existing visual tracking systems struggle to maintain long-term, accurate tracking due to frequent identity association errors, which lead to extensive manual correction and limit research scalability. This paper introduces mTrack, an RFID–vision hybrid mouse tracking system that leverages the precise identification capability of UHF RFID to assist the visual tracker, enabling long-term, self-correcting, and high-accuracy mouse tracking. Our experiments demonstrate that mTrack can track up to ten mice simultaneously with over 99.23% identification accuracy and a 0.4 cm 99th-percentile localization error, reducing error rate by more than 40x compared with visual tracking systems. Our field studies indicate that mTrack can sustain this performance for over two hours and be seamlessly integrated into existing animal behavior research workflows. The code and dataset are open-sourced at https://github.com/SOAR-PKU/mTrack.

CCS Concepts

• **Computer systems organization → Embedded and cyber-physical systems**; • **Applied computing → Life and medical sciences**.

*Also with Key Laboratory of High Confidence Software Technologies, Ministry of Education (PKU).
†Corresponding author: chenren@pku.edu.cn

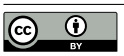

SenSys '26, Saint Malo, France

ACM ISBN 979-8-4007-2309-4/26/05
https://doi.org/10.1145/3774906.3800473

Keywords

Multi-Object Tracking, Social Behavior Analysis, Wireless Sensing

ACM Reference Format:
Xingyuming Liu, Bo Liang, Haobo Wang, Zhonghao Li, Qirui Liu, Yanxue Xue, Yunhuai Liu, Chenren Xu. 2026. mTrack: Enabling Long-Term Mouse Social Behavior Analysis through RFID-Vision Hybrid Tracking. In *ACM/IEEE International Conference on Embedded Artificial Intelligence and Sensing Systems (SenSys '26), May 11–14, 2026, Saint Malo, France.* ACM, New York, NY, USA, 14 pages. https://doi.org/10.1145/3774906.3800473

1 Introduction

Mice are widely used as preclinical models to investigate human diseases due to their genetic similarities to humans [57]. Studying social behavior among mice provides critical insights into drug screening, depression assessment, and gene function research [33, 60, 62]. These studies help identify therapeutic targets, understand neurobiological mechanisms, and develop interventions for human conditions such as autism, schizophrenia, and mood disorders [33].

Social behavior study requires accurate and continuous tracking of individuals within a mouse group, with a particular focus on *maintaining their identities over time.* Modern visual tracking methods often rely on differences in visual appearance and motion continuity for both tracking and identification [6, 74, 79]. However, mouse tracking poses two fundamental challenges to the current visual trackers:

- *Undistinguishable Appearance.* In behavioral experiments, most mice share similar genetic backgrounds, resulting in nearly identical appearances [41]. As a consequence, it is hard to distinguish individuals based on appearance.
- *Complex Motion Pattern.* Movement of mouse is rapid (instantaneous speeds up to 1.68 m/s [25]) and erratic, and frequent

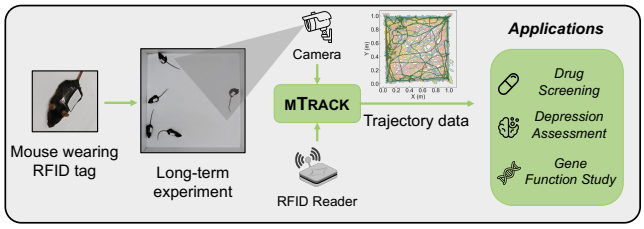

Figure 1: mTrack achieves highly accurate mouse tracking, enabling biologists to study the long-term social behavior of mice effectively.

clustering and interaction between mice lead to occlusion, challenging motion-based identity prediction.

These factors collectively contribute to frequent *identity association errors* [44], where visual trackers assign the wrong identity to the tracked mouse. Worse still, existing visual trackers lack an error correction mechanism – once an identity is misassigned, the error propagates indefinitely. Over time, nearly all tracked mice will eventually be misidentified. Specifically, the state-of-the-art (SOTA) visual tracker can track only up to four mice, with no guarantees of identity persistence, relying on human intervention for quality checks and corrections, which significantly increases labor efforts [46, 51, 54, 55]. Our pilot study (§2.1) demonstrates that a SOTA tracker [79] can maintain correct identity tracking for no more than one minute. The limitation of tracking capacity has constrained most current social behavior studies to dyadic interactions between two mice, while research on the richer and more complex social dynamics within larger groups remains scarce [72].

A complementary approach for identification during tracking is to attach visual tags on the mouse, such as AprilTags [50] and QR codes [3, 15]. By recognizing the visual tags on mice, their identities can be easily determined. However, small visual tags (*e.g.,* 1 x 1 cm) matching the size of mice are prone to staining from food residue or hair during experiments and ineffective in low-light conditions [3, 15], highlighting the need for alternative identification methods beyond visual cues.

One promising alternative is Ultra-High-Frequency (UHF, 860-960 MHz) RFID, which offers non-line-of-sight (NLOS) identification capabilities with extended range (up to 10 m) and high-speed interrogation (1000+ reads/sec) [29]. Unlike visual tags, the identification of UHF RFID is unaffected by lighting conditions or physical obstructions. Particularly, UHF RFID has demonstrated its potential for object identification when fused with visual data in applications such as smart retail and human-object interaction [22, 36, 43]. The fusion leverages the complementary strengths of visual tracker and UHF RFID: Visual tracker excels at precise object detection and localization but struggles with identification, while UHF RFID provides accurate, long-range identification and phase data for coarse positional information. By integrating these modalities, a matching algorithm matches the visual trajectory of an object with a specific UHF RFID tag, enabling accurate identification and correction of the visual trajectory.

In this paper, we present mTrack, the first mouse tracking system that integrates visual tracking with UHF RFID technology to enable long-term, self-correcting, and high-accuracy mouse tracking. By attaching UHF RFID tags to individual mice, we provide them with physical identities for accurate identification. mTrack achieves highly accurate and robust tracking by addressing three key challenges. The first is *reliability* — maintaining high identification accuracy over long-term experiments. Scientific research requires exceptionally high accuracy (*e.g.,* 97%) across multi-hour studies [16, 41, 49]. Existing UHF RFID–vision systems [22, 36, 43] work well only in constrained motion patterns (*e.g.,* simple linear trajectories or repetitive, predictable movements) commonly found in application scenarios such as smart retail, where tagged items are moved along fixed paths, or human–computer interaction, where participants perform predefined gestures in front of cameras. In these settings, visual trackers rarely make association errors. In contrast, mice move randomly and are frequently occluded, leading to frequent association errors. In this case, RFID needs to provide not only identification but also correction of visual tracker errors across frames. Unlike prior work that relies on the visual tracker to provide already-correct trajectories, mTrack is designed to actively detect and fix association errors. To achieve this, mTrack introduces an RFID-vision trajectory matching algorithm that identifies and corrects the visual trajectories by monitoring the matching scores with UHF RFID phase sequences.

During the clustering and interaction of mice, visual trackers suffer from frequent identity association errors, which presents the second challenge — *timeliness — to resolve frequent identity association errors in time.* The short interval of identity association errors imposes a strict deadline for the matching algorithm. mTrack must identify the trajectory before subsequent association errors compound existing ambiguities. To address this, we design a tracklet identity manager with two key features. First, it infers possible identities per trajectory using visual context, reducing the number of matching tag candidates and accelerating the matching process. Second, it tolerates some untimely matches by leveraging current match results to retroactively correct past association errors.

Social behavior studies require a reasonable number of subjects (*e.g.,* more than five) to enable the investigation of complex social interactions [10, 69], leading to the final challenge — *scalability — tracking as many mice as possible.* As the number of mice increases, the read rate per tag drops significantly due to channel contention in RFID systems (halving when scaling from two to ten tags), slowing the convergence of the matching algorithm. In contrast to reading all tags indiscriminately, reading resources must be allocated efficiently by prioritizing tags that require more frequent updates. In mTrack, we identify that tags not yet matched to any trajectory and high-mobility tags should be prioritized for reading. Based on this insight, we design an RFID reading scheduler that dynamically allocates resources based on matching status and mobility.

We implement mTrack using commodity hardware and demonstrate its ability to meet key biological tracking requirements (Tab. 1). mTrack enables continuous tracking of ten mice with 99.23% accuracy, eliminating the need for manual correction compared to visual trackers. Compared to previous UHF RFID-vision systems, mTrack maintains high accuracy under unpredictable mouse motion and improves the tracking capacity from six to ten targets. In the field study, mTrack achieved 98.7 ± 0.2% accuracy with ten mice over

Table 1: Comparison of mTrack with state-of-the-art tracking systems.

Modality	System	Tracking Capacity (≥ 5 subjects)	Mobility Support (Unpredictable motion)	Identification Accuracy (≥ 97%)[1]	Localization Precision (≤ 1 cm)[3]
RFID Systems	PinIt [65]	Yes (1 tag)	No (Static targets)	N/A[2]	No (11.2 cm)
	MobiTagbot [59]	Yes (20 tags)	No (Static targets)	N/A[2]	No (3–4 cm)
	RF-IDraw [66]	No (1 tag)	No (Drawing fixed characters)	N/A[2]	No (19 cm)
	Tagoram [75]	No data reported	No (Conveyor belt motion)	N/A[2]	No (12.3 cm)
Vision Systems	idtracker.ai [55]	No (4 mice)	Yes (Free moving animals)	No (Need manual correction)	Yes (<1 cm)
	DeepLabCut [46]	No (3 mice)	Yes (Free moving animals)	No (Need manual correction)	Yes (<1 cm)
RFID-Vision Hybrid Systems	ID-Match [36]	Yes (5 tags)	No (Simple linear motion)	No (95%)	Yes (<1 cm)
	RF-Camera [43]	No (4 tags)	No (Drawing fixed characters)	No (~85%)	Yes (<1 cm)
	TagView [22]	Yes (6 tags)	No (Simple linear motion)	No (96%)	Yes (<1 cm)
	mTrack (Ours)	**Yes (10 tags)**	**Yes (Free moving mice)**	**Yes (99.23%)**	**Yes (<1 cm)**

[1] The accuracy requirement (97%) is based on results reported by previous animal behavior studies based on mouse tracking [16, 41, 49].
[2] "N/A" indicates that the metric is not applicable. RFID systems inherently provide ID and do not require a separate association step to determine ID.
[3] The median localization error is presented. Sub-centimeter localization is typically achieved by visual-modality methods, provided identity errors are disregarded.

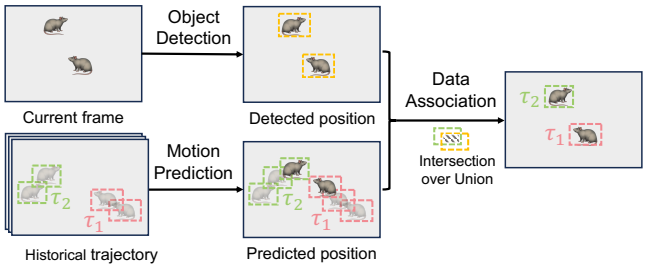

Figure 2: Visual tracking pipeline.

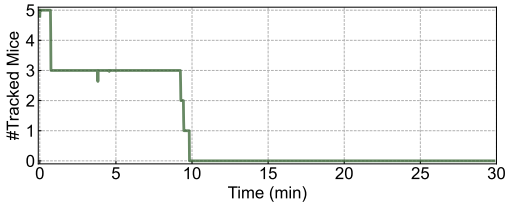

Figure 3: Visual tracker fails to track 5 mice.

two hours, fulfilling the requirements of classic behavioral studies [12]. Our contributions can be summarized as:

- We present mTrack, the first UHF RFID-vision hybrid system capable of accurately tracking multiple mice simultaneously over extended periods, addressing the limitations of existing visual tracking methods.
- We design a novel RFID–vision fusion framework extending RFID–vision tracking to scenarios with frequent identity association errors. It integrates an RFID–vision trajectory matching algorithm (§4), a tracklet identity manager (§5), and an RFID reading scheduler (§6).
- We collaborate with biologists to conduct field studies using mTrack, demonstrating its ability to support long-term mouse tracking and integrate into social behavior analysis workflows.

This work does not raise any ethical concerns, and all biology-related experimental procedures were reviewed and approved by the Institutional Review Board.

2 Background and Pilot Study

Current biological research primarily relies on visual solutions for mouse tracking. In this section, we provide a primer on visual tracking and present a pilot study to evaluate the performance of vision-based mouse tracking.

2.1 Visual Tracking Primer and Evaluation

Task Definition. Mouse tracking is a Multi-Object Tracking (MOT) problem, which aims to detect and maintain continuous trajectories of multiple objects in a video sequence. Each object is represented by a bounding box, defined by its center coordinates, width, and height. The output of MOT is a set of *tracklets*, where each tracklet is an ordered sequence of bounding boxes describing an object's movement over time. Each tracklet is denoted as τ_k, where k is the unique ID assigned by the visual tracker. MOT follows the Track-by-Detection framework [6, 74, 79], which consists of two main steps as shown in Fig. 2:

- *Detection*: It detects and localizes objects in each frame, outputting bounding boxes.
- *Association*: It associates the currently detected bounding boxes to existing tracklets by predicting their future positions (e.g., using a Kalman filter) and computing similarity metrics like intersection-over-union (IOU). Low-similarity associations are rejected, and unassociated detections initialize new tracklets.

To assess the effectiveness of visual tracking, we conduct a pilot study using a SOTA visual tracker ByteTrack [79] for tracking, combined with YOLOv8 [32] for object detection. We analyze a 30-minute video featuring five mice. As shown in Fig. 3, the visual tracker lost tracking of two mice within the first minute and failed to track all mice within ten minutes, demonstrating its inability to maintain long-term tracking.

To further investigate the source of errors, we analyze the widely adopted Higher Order Tracking Accuracy (HOTA) metrics [44] to determine whether the errors stem from detection or association:

Detection Accuracy. It measures how well an object detector localizes subjects (mouse) using bounding boxes. The results show YOLOv8 exhibited high accuracy of more than 99% for the entire video , with occasional errors during occlusions or close interactions. This high accuracy confirms that detection error is not the primary issue in mouse tracking.

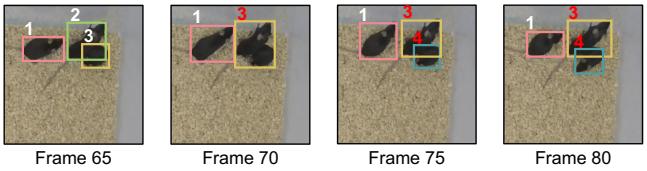

Figure 4: An example of association error.

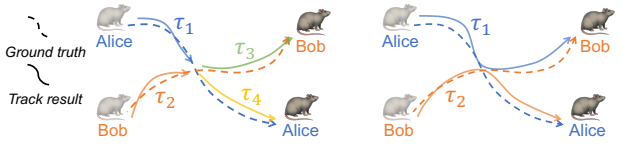

(a) Fragmentation. **(b) ID switch.**

Figure 5: Illustration of association errors.

Association Accuracy. It evaluates how well a tracker associates detected bounding boxes with their corresponding tracklets across frames. The results show that ByteTrack's association accuracy is notably low, at only 37.5%, indicating that over 60% of the bounding boxes are incorrectly assigned. An example of association error is illustrated in Fig. 4. In Frame 70, the two mice move closely and cannot be correctly detected separately. Then, when they separate in Frame 75, Mouse 2 is recognized as Mouse 3, and Mouse 3 is reinitialized as Mouse 4. These association errors make visual tracking systems fail to keep correct tracking for the long term.

Appearance Based Re-identification. One approach to mitigate association errors is visual appearance-based re-identification (Re-ID), which leverages appearance differences to distinguish tracked objects. To evaluate its feasibility for mouse tracking, we construct a dataset of 1,000 labeled images from five mice and finetune the widely used Omni-Scale Network (OSNet) [80]. The model achieves a low top-1 accuracy of just 37.3%, meaning that in over 60% of cases, it incorrectly identifies two different mice as the same individual. These results confirm that appearance-based Re-ID is unreliable for distinguishing between mice.

2.2 Understanding Association Errors

To better understand the association errors, we explain the root causes of association errors and evaluate how frequently they occur.

Reasons for Association Errors. Association errors occur when the tracking system incorrectly assigns identities to detected tracklets. Based on our observations and previous work on assessing MOT performance [38, 53], these errors manifest in two primary forms, as shown in Fig. 5: 1) Fragmentation. The ground truth trajectory of a single identity is fragmented into multiple tracklets. 2) ID switch. The ground truth identities of two or more tracklets are incorrectly interchanged. These errors primarily stem from the limitations of motion-based association in visual tracking, as it relies on movement continuity rather than unique physical identifiers, making association errors inevitable when mice interact closely or occlude one another.

Frequency of Association Errors. To quantify the frequency of association errors, we analyzed the cumulative distribution function (CDF) of the time intervals between consecutive association errors (Fig. 6). While the average interval between association errors is

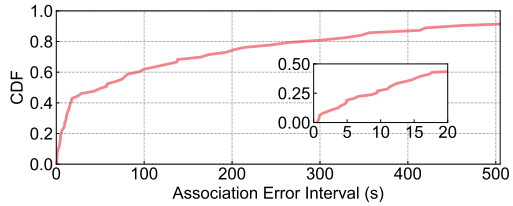

Figure 6: CDF of association error time intervals.

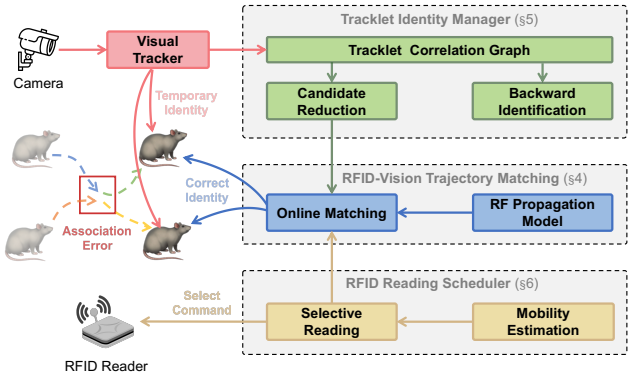

Figure 7: mTrack overview.

over two minutes, 20% of errors occur within just 5.4 seconds. This distribution reflects the social behavior patterns of mice: they act independently most of the time, but occasionally gather and interact, triggering frequent association errors. The tracking system is expected to be able to recognize and resolve association errors within this time margin, which is very challenging.

Takeaway. The results suggest that association errors — not detection limitations — pose the greatest challenge to long-term mouse tracking. These errors are frequent in visual tracking and cannot be solved by appearance-based Re-ID. This aligns with findings from [78], which reports that visual trackers exhibit significant performance degradation when applied to animal datasets such as AnimalTrack [78], compared to human/vehicle-focused datasets like MOT17 [47]. A permanent and reliable identification method beyond visual features is necessary to address association errors, which motivates our use of UHF RFID to provide physical identifiers for assisting the identification process.

3 Overview

mTrack addresses long-term mouse tracking challenges in biological studies by synergizing UHF RFID identification with visual trajectory data. As illustrated in Fig. 7, our design comprises three key components. First, we design an RFID-vision trajectory matching algorithm (§4) that performs continuous matching with confidence checks, enabling high matching accuracy. Second, we design a graph-based tracklet identity manager (§5) that propagates identities across tracklets. Through candidate reduction and backward identification mechanisms, this module accelerates the convergence of the matching algorithm and tolerates some failed matches. Third, we develop an RFID reading scheduler (§6) to allocate limited reading resources efficiently, mitigating the effects of contention-induced reductions in reading rate when scaling to

more mice. Together, these components enable mTrack to achieve long-term, self-correcting, and high-accuracy mouse tracking in biological research.

4 RFID-Vision Trajectory Matching

In this section, we formalize the problem of UHF RFID and vision hybrid tracking as a tracklet matching problem. Then we introduce how mTrack ensures a highly reliable matching with a carefully designed similarity quantification based on the RFID signal model and an online matching algorithm.

4.1 Problem Definition

In our experiment setup, each mouse is physically equipped with a unique UHF RFID tag. The task is to match visual tracklets with their corresponding RFID tags. Let $\tau = \{\tau_1, \tau_2, \ldots, \tau_M\}$ denotes the set of visual tracklets and $R = \{r_1, r_2, \ldots, r_N\}$ is the set of RFID tags. In practice, $M \geq N$ due to the fragmentation errors (Fig. 5a) in the tracking process. The objective is to establish a mapping $\sigma : \tau \rightarrow R$ that optimally associates tracklets with their physical identifier – RFID tags.

The RFID reader queries the tags in sequence, and the tags backscatter the signal to reply. For each RFID tag r_j, we observe a signal phase sequence $\Theta_j = \left[\theta_j(t_1), \theta_j(t_2), \ldots, \theta_j(t_K)\right]$ at discrete timestamps t_k. Positions P_i for tracklet τ_i are aligned to RFID timestamps via linear interpolation: $P_i = [p_i(t_1), p_i(t_2), \ldots, p_i(t_K)]$, where $p_i(t_k)$ is the center position of the bounding box of tracklet τ_i at time t_k.

Since the phase is dominated by the tag-antenna distance, which can be derived from the tracklet positions, we can predict the phase values $\hat{\Theta}_i$ related to tracklet τ_i by a signal propagation model $\mathcal{F}$:

$$\begin{aligned}\hat{\Theta}_i &= \left[\hat{\theta}_i(t_1), \hat{\theta}_i(t_2), \ldots, \hat{\theta}_i(t_K)\right] \\ &= [\mathcal{F}(p_i(t_1)), \mathcal{F}(p_i(t_2)), \ldots, \mathcal{F}(p_i(t_K))]\end{aligned} \tag{1}$$

Formally, the matching problem is to find a mapping $\sigma : \tau \rightarrow R$ that maximizes aggregate similarity between the predicted phases of tracklets and the measured phases of RFID tags:

$$\max_{\sigma} \sum_{i=1}^{M} \mathcal{S}(\mathcal{F}(P_i), \Theta_{\sigma(i)}) \tag{2}$$

where $\mathcal{S}(\cdot)$ quantifies the similarity between the phase sequences.

4.2 Algorithm Design

Signal Propagation Model. The RF phase is determined by the propagation distance but is also influenced by hardware characteristics and environmental multipath effects:

$$\theta = \left(\frac{4\pi d}{\lambda} + \theta_{hw} + \theta_{env}\right) \mod 2\pi \tag{3}$$

where d is the tag-to-antenna distance, λ is the carrier wavelength, θ_{hw} is the phase offset caused by hardware characteristics, and θ_{env} is the phase offset caused by multi-path effects [28].

Due to the unknown phase offset θ_{hw} and θ_{env}, it is hard to predict phases $\hat{\Theta}_i$ from tracklet positions P_i. As an alternative, we take the phase difference between the adjacent measurements

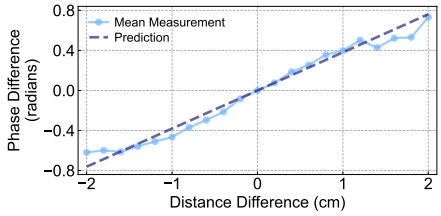

Figure 8: Empirical verification of the phase model.

to calculate the similarity, assuming that θ_{hw} and θ_{env} are nearly identical for adjacent measurements:

$$\Delta\hat{\theta}_i(t_k) = \hat{\theta}_i(t_k) - \hat{\theta}_i(t_{k-1}) = \frac{4\pi\Delta d}{\lambda} \mod 2\pi \tag{4}$$

where Δd is the change in the tag-to-antenna distance between t_k and t_{k-1}, which can be predicted from tracklet positions and calibrated antenna locations. We validate our phase model by collecting 30 minutes of motion data from five mice and analyzing the phase differences across varying Δd. The mean measured phase differences closely match the predictions, confirming that our assumption holds (Fig. 8).

Similarity Quantification. We take the Manhattan distance between the predicted and the measured phase difference to measure the similarity:

$$\mathcal{S}(\hat{\Theta}_i, \Theta_j) = -\frac{1}{K-1} \sum_{k=1}^{K-1} |\Delta\hat{\theta}_i(t_k) - \Delta\theta_j(t_k)| \tag{5}$$

Online Matching Framework. With the similarity quantification, a direct approach to solve the matching problem 2 is using a global optimization-based method [22]. However, this approach is sensitive: a few mismatches can skew the entire solution, leading to low accuracy, as confirmed by our comprehensive evaluation in §8.2. Instead, we propose an online matching framework that only accepts high-confidence matches to minimize mismatches. mTrack maintains the matching status for the active tracklets and tags and continuously updates the matching scores *between unmatched tracklets and tags*. When a score meets predefined matching criteria, mTrack accepts the match and updates the tracklet and tag to *matched status*.

The matching criteria are defined as follows. Let M be the matching score matrix, where $M_{i,j}$ represents the matching score between tracklet τ_i and tag r_j, $M_{i,j} = \mathcal{S}(\hat{\Theta}_i, \Theta_j) \leq 0$. A tracklet τ_i is considered matched with tag r_j if the following two conditions are simultaneously satisfied:

(1) **Maximal Condition:** The matching score for tag r_j with tracklet τ_i is significantly higher than the matching scores with other tracklets.
$$M_{k,j} < (1+\alpha)M_{i,j} \quad \forall k \neq i$$
(2) **Stable Condition:** The matching score for tracklet τ_i with another tag r_k is significantly lower than the maximal matching score of r_k.
$$M_{i,k} < (1+\alpha)\max_{u} M_{u,k} \quad \forall k \neq j$$

where $\alpha > 0$ since the matching scores are negative.

Online Quality monitor. Even with high-confidence matches, errors can still arise. These primarily occur in two scenarios: First,

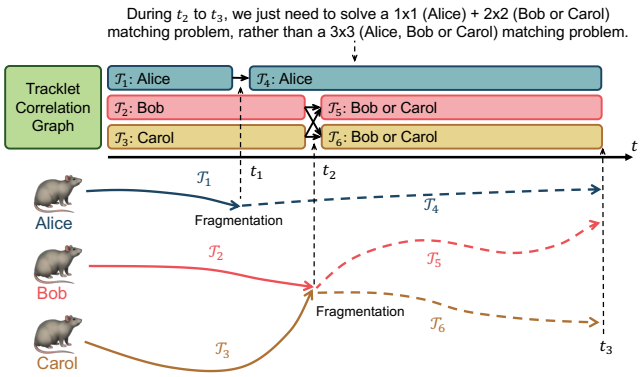

Figure 9: A toy example to show how the tracklet identity manager reduces the matching candidates.

the matching algorithm still has a small probability of mismatch. Second, and more subtly, even correctly matched tracklets can later suffer from ID switches within the visual tracker, as illustrated in Fig. 5b. These mismatches propagate across subsequent frames, causing unpredictable errors if left unaddressed.

To address this, we implement an online quality monitor that continuously monitors the matching scores of *matched tracklets and tags*. Suppose a tracklet τ_i is matched with tag r_j, we flag potential mismatch when the maximal and stable conditions are significantly violated, *i.e.,* $M_{i,j} < (1+\beta)\max_k M_{k,j}$ and $M_{i,k} > (1+\beta)\max_u M_{u,k}$ for some $k \neq j$, where β is a positive parameter. The monitor submits reading requests in a round-robin manner to minimize reading resource usage. When a potential mismatch is flagged, the tracklet and tag are reverted to unmatched state, allowing the matching algorithm to correct the errors.

Scale to Multi-frequency and Multi-antenna. We use frequency hopping across 50 ISM channels (902–928 MHz) at 200 ms intervals to enhance resistance to multipath interference [59]. Since tags show different phase offsets on each channel, we compute phase differences using adjacent measurements within the same channel. To minimize blind spots, we adopt a multi-antenna setup and sum up phase similarity across antennas.

5 Tracklet Identity Manager

As discussed in the pilot study §2.1, narrow error association intervals impose strict temporal constraints, requiring timely identification to prevent error accumulation. To address this challenge, we propose a tracklet identity manager comprising two key techniques: candidate reduction optimization §5.2 and backward identification §5.3. The core data structure behind these techniques is the tracklet correlation graph §5.1. Together, the manager accelerates matching and resolves potential matching failures.

5.1 Tracklet Correlation Graph

The tracklet correlation graph is a data structure that records the generation relationships between tracklets – indicating which tracklets are generated from the association errors of others. It is a directed graph structure $G = (V, E)$, where nodes represent visual tracklets and edges represent successive relationships. We formally define the graph as follows:

Nodes. Each node $\tau_i \in V$ represents an individual visual tracklet. Node attributes are defined as:

$$\textbf{Attributes}(\tau_i) = \{S, TagSet, P_{\text{start}}, P_{\text{end}}, t_{\text{start}}, t_{\text{end}}\}$$

- **Status** $S \in \{0, 1\}$ indicates identified state (0=Unidentified, 1=Identified). Initialized to 0, updated to 1 after a successful match.
- **TagSet** contains possible identities for τ_i. Reduces to a singleton after a successful match.
- **Start and End Position** ($p_{\text{start}}, p_{\text{end}}$) denote the spatial coordinates where the tracklet begins and ends.
- **Start and End Time** ($t_{\text{start}}, t_{\text{end}}$) record the timestamps when the tracklet begins and ends.

Edges. A directed edge $e_{s\to d} \in E$ connects parent node τ_s to child node τ_d, indicating that tracklet τ_d generates from the termination of tracklet τ_s and inherits all the identity candidates of τ_s:

$$TagSet(\tau_d) = \bigcup_{e_{s\to d}\in E} TagSet(\tau_s)$$

Graph Construction. When there is a new tracklet initialized from the visual tracker, it is added to the graph with $S = 0$ (Unidentified). Edges are created based on spatiotemporal proximity between tracklets: a new tracklet should generate from a *recently* terminated tracklet that ended *near* the new tracklet's start position. Let S_{init} and S_{term} denote the sets of recently initialized and terminated tracklets within a time window Δt. When a new tracklet $\tau_{\text{init}} \in S_{\text{init}}$ is initialized, we search for a recently terminated tracklet $\tau_{\text{term}} \in S_{\text{term}}$ for which $\|p_{\text{start}}(\tau_{\text{init}}) - p_{\text{end}}(\tau_{\text{term}})\| \leq d_{\max}$, where $d_{\max}$ represents the distance threshold. If these conditions are met, an edge $e_{\tau_{\text{term}}\to\tau_{\text{init}}}$ is added to the graph, indicating that τ_{init} inherit the identity candidates from τ_{term}.

5.2 Candidate Reduction

To reduce the matching time, we leverage the idea that matching time scales with the matching problem size. Instead of matching tracklets with all unmatched tags, we infer possible identities of tracklets to reduce candidates. We first detail our algorithm design and then illustrate it with a toy example.

Algorithm Design. To maintain the possible identities of nodes, identities are propagated along the edges of the graph. When an edge $e_{s\to d}$ is added to the graph, we propagate the identities of τ_s to the τ_d:

$$TagSet(\tau_d) = TagSet(\tau_d) \cup TagSet(\tau_s)$$

By propagating identities in this manner, we restrict the matching space of a tracklet to its *TagSet*, rather than attempting to match it with all unmatched tags. Formally, we set the matching score matrix as follows:

$$\begin{cases} M_{i,j} = \mathcal{S}(\hat{\Theta}_i, \Theta_j), & \text{if} \quad r_j \in TagSet(\tau_i) \\ M_{i,j} = -\infty, & \text{if} \quad r_j \notin TagSet(\tau_i) \end{cases}$$

Toy Example. As shown in Fig. 9, tracklet τ_1 encounters a fragmentation error and terminates, with a new tracklet τ_4 initialized at time t_1. Later, τ_2 and τ_3 are terminated due to another fragmentation error with new initialized tracklets τ_5 and τ_6 at t_2. The tracklet

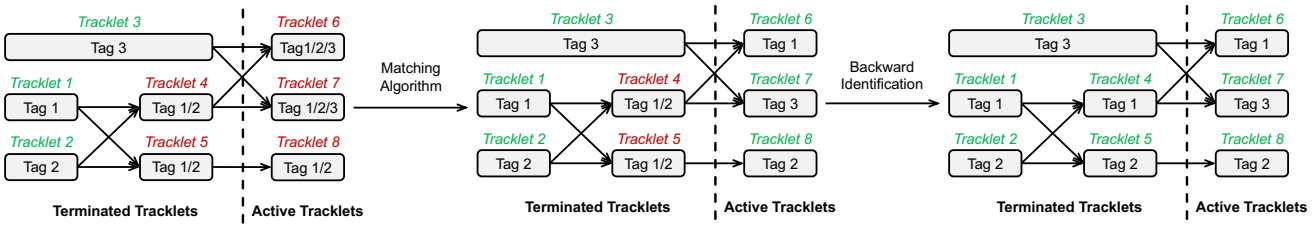

Figure 10: A toy example to show how backward identification solves historical errors.

identity manager propagates identities from terminated tracklets to their successors. Based on the tracklet correlation graph, we solve a 1×1 (Alice) + 2×2 (Bob or Carol) matching problem instead of a full 3×3 (Alice, Bob, or Carol) matching problem, significantly reducing the matching time.

5.3 Backward Identification

Some association errors occur within very short intervals (even less than one second), as shown in the pilot study (Fig. 6), resulting in short tracklets that are inherently challenging to identify before termination. Are these terminated nodes no longer identified? No. In this section, we introduce the backward identification technique, which can recover these historical errors based on the matching results of their successor nodes.

Algorithm Design. Suppose an unidentified tracklet τ_i and all its successive nodes $\{\tau_{i_1}, \ldots, \tau_{i_n}\}$. The backward identification proceeds as follows:

(1) **Successor monitoring.** It checks the status S of all successor nodes. Once all successor nodes are identified, move to Step 2.
(2) **Backward identification.** It backward propagates the identity of the successor nodes, and updates $TagSet(\tau_i)$ as follows:

$$TagSet(\tau_i) = TagSet(\tau_i) \cap \left(\bigcup_{k=1}^{n} TagSet(\tau_{i_k}) \right) \tag{6}$$

If the size of $TagSet(\tau_i)$ reduces to 1, the tracklet τ_i is successfully identified. If the size remains greater than 1, the identity of τ_i cannot be uniquely determined.

Although the algorithm's success is not theoretically guaranteed, it resolves most match failures in practice, as association errors rarely accumulate to a level of complexity that prevents backward identification from working.

Toy Example. Fig. 10 illustrates an example, the tracklet τ_4 is terminated before it can be identified by the matching algorithm, due to an association error between τ_3 and τ_4. Then, tracklets τ_6 and τ_7 are generated from τ_3 and τ_4, inheriting their potential identities. When τ_6 and τ_7 are matched with Tag 1 and Tag 3 in the future time, respectively, we deduce that identity Tag 1 must originate from τ_4, as τ_4 is the only predecessor node of τ_6 with Tag 1 in its possible identity set. Thus, τ_4 is identified as Tag 1. Similarly, when tracklet τ_8 is identified, τ_5 is identified as Tag 2 using the same approach.

6 RFID Reading Scheduler

6.1 Insights

mTrack's matching algorithm requires multiple tag readings for high-confidence matches. As the number of tags increases, each match needs significantly more readings to converge (Fig. 11), but the per-tag read rate drops by over half when scaling from two to ten tags due to contention (Fig. 12). These factors slow matching convergence as the number of mice grows. To address this, we design an RFID reading scheduler based on two key insights:

- *Prioritizing Unmatched Tags.* Once a tag is matched, frequent reads are unnecessary, allowing the reader to focus on unmatched tags.
- *Prioritizing High-Mobility Tags.* Slow-moving tags exhibit minimal phase variation and require lower read rates, while fast-moving tags need higher read rates to avoid phase ambiguity [40].

Building on these insights, we propose a two-stage reading scheduler that dynamically allocates reading resources to unmatched tags based on mobility (Fig. 13): Stage 1 reads all unmatched tags and identifies high-mobility tags from phase data. Stage 2 focuses on these high-mobility tags. Next, we detail two key algorithms in the scheduler: mobility estimation (§6.2) and mask generation (§6.3).

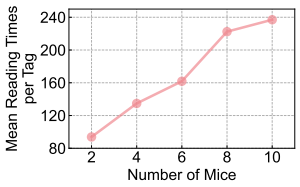

Figure 11: Reading times per tag for a match.

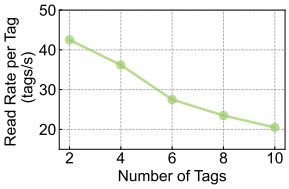

Figure 12: Tag reading rates.

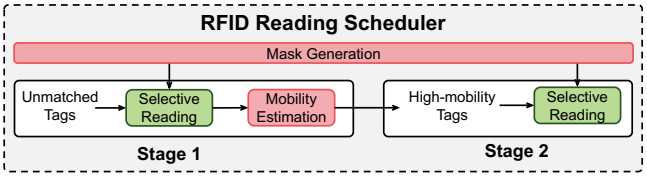

Figure 13: RFID reading scheduler design.

6.2 Mobility Estimation

To identify the high-mobility tags, the scheduler must infer the tag mobility first. It may seem that mobility can be inferred from visual clues. However, tags requiring reading are precisely those not yet matched to tracklets, making their corresponding tracklets and mobility hard to determine. Therefore, in our design, we infer the tag mobility from the RFID phase data collected in Stage 1.

RFID phase differences effectively indicate tag mobility. A stationary tag has phase differences close to zero, whereas a tag moving toward (or away from) the antenna consistently shows negative (or positive) phase differences. However, a single phase difference is

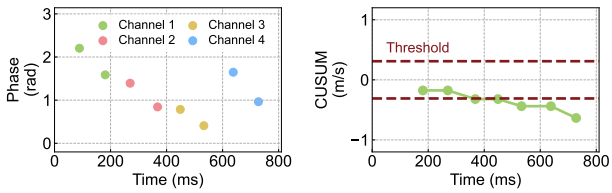

Figure 14: Phase and CUSUM for a mouse towards the antenna.

sensitive to noise, so we develop a cumulative sum (CUSUM)-based method for robust mobility estimation. Let the phase differences for a tag be denoted as $[\Delta\phi_1, ..., \Delta\phi_n]$ measured over time intervals $[\Delta t_1, ..., \Delta t_n]$. The instantaneous speed at time i is estimated by $v_i = \frac{\Delta\phi_i \lambda}{4\pi\Delta t_i}$. We compute the cumulative speed over all measurements as $s = \sum_{k=1}^{n} v_k$. If the absolute cumulative speed exceeds a predefined threshold C, *i.e.,* $|s| > C$, we classify the tag as having high mobility (Fig. 14).

6.3 Mask Generation

To selectively read target tags, the scheduler uses the `Select` command defined in the EPC UHF Gen II Air protocol [24]. To select a target tags set $\mathcal{S}$, one could select each tag individually. However, practical deployments are constrained by N_{max} — the maximum number of `Select` commands allowed per inventory round (two to five in commercial readers [5, 30]). To address this, we propose a two-phase (select–then–deselect) mask generation algorithm that ensures full target coverage with minimal commands.

Select with GEN II. The EPC UHF Gen II Air Interface Protocol [24] defines the `Select` command, which allows an RFID reader to choose a subset of tags for the subsequent inventory round. The `Select` command takes four parameters relevant to our design: `Mask`, `MemBank`, `Pointer`, and `Action`. Here, `Mask` is a bit string for memory comparison, `MemBank` specifies the memory bank, `Pointer` specifies the start position in that bank, and `Action` specifies whether matching tags are selected or deselected. The `Select` command can be formally expressed as:

$$S(\texttt{Mask}, \texttt{Pointer}, \texttt{Action}),$$

where `MemBank` defaults to EPC memory in our setting.

Mask Generation Algorithm. Mask generation can be formulated as a set covering problem [40], which is known to be NP-hard [9]. To solve this problem, we implement a greedy algorithm for mask generation. Our algorithm operates in a "select first, then deselect" manner, comprising the following steps:

(1) **Mask Candidate Generation.** Given a set of n tags with EPC of length L, we first generate a raw mask candidate set $\mathcal{M}$ with the substrings of the EPCs:

$$\mathcal{M} = \{m = \text{EPC}_i[p:q] \mid p, q \in [0, L), p < q\}.$$

where EPC_i is the EPC of tag i, and m is a mask candidate that matches the EPC from position p to position q. The maximum size of $\mathcal{M}$ is $nL(L+1)/2$. We then reduce the size of $\mathcal{M}$ by retaining only one representative mask for each group of masks that match the same set of tags, resulting in a smaller set $\mathcal{M}'$.

(2) **Target Tags Selection.** The algorithm selects the mask candidate from $\mathcal{M}'$ that covers all the target tags while minimizing the selection of non-target tags. The success of this step is guaranteed by the EPC optimization introduced later.

(3) **Non-target Tags Deselection.** The algorithm iteratively deselects the non-target tags that are selected in Step 2. In each iteration, it chooses the mask candidate that deselects the maximum number of non-target tags without affecting the selected target tags. This process continues until all non-target tags are deselected or the `Select` limit is reached.

EPC Optimization. The performance of the mask generation algorithm depends on the EPC of the tags. To enable selection of all target tags using as few `Select` instructions as possible while minimizing the inclusion of non-target tags, we inject some bits in the suffix of the EPC, referred to as *GroupID*. We define two types of bits in *GroupID*:

- *Universal bit*: All tags set this bit to one, ensuring that Step 2 of the mask generation algorithm selects all target tags.
- *Bundling bit*: A carefully designed bit vector proposed in previous work [42] for high efficient select operation.

Using the mask generation algorithm and carefully designed EPC IDs, we can select all target tags within a single inventory round.

7 Implementation

Hardware. As shown in Fig. 15, we implement mTrack using commercial off-the-shelf (COTS) hardware. Specifically, we use an Impinj R700 RFID reader [29] with four linearly polarized antennas and a camera (1920 × 1080 resolution, 30 FPS) for visual tracking. Following the common open-field setup [18], experiments are conducted in a customized 1 m × 1 m mouse cage, with four antennas along the perimeter and an overhead camera for a bird's-eye view. The cage is set at a height of 0.5 m to minimize ground multipath reflections. The reader and camera are connected to a laptop with an Intel Core i5-13500HX processor, 16 GB of RAM, and an NVIDIA GeForce RTX 4060 Laptop GPU.

Software. The laptop communicates with the RFID reader via the Low-Level Reader Protocol (LLRP) [26], using software developed with the Octane SDK [31] in C#. Camera data is captured using OpenCV [7]. The visual tracker is based on the open-source implementation from Ultralytics [63], incorporating YOLOv8 for object detection and ByteTrack for visual tracking. All tracking-related algorithms are implemented in Python.

Tag Installation. Given the small body size of lab mice, we use 1.5 cm × 2.5 cm UHF RFID tags integrated with the UCODE 9xe chip [48] to minimize physical burden. However, small tags have shorter read range, especially on biological surfaces, which absorb electromagnetic waves because of high water content; in our case, range drops to 30 cm. To address this, we add a 1 mm foam layer between the tag and biological surface, improving impedance matching by reducing interaction with this high-loss medium [17, 34]. This extends the reading range to about 1.5 meters, sufficient for our setup. The tag, including foam, weighs only 0.1 g, much lighter than a commercial metal/plastic ear tag (0.2–0.7 g) [1, 56].

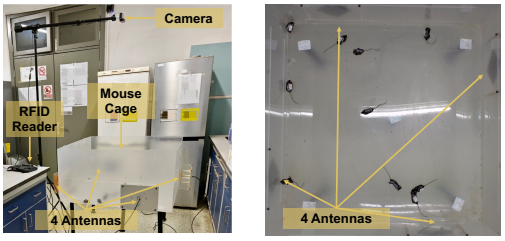

(a) Plain view. (b) Aerial view.

Figure 15: Experimental setups.

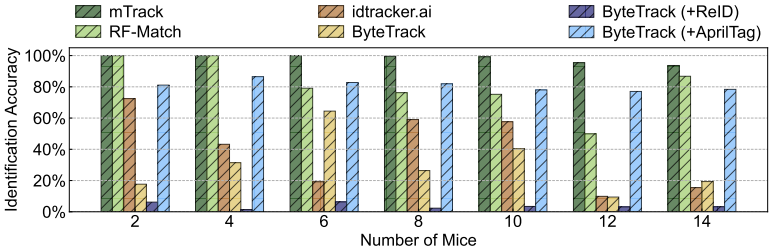

Figure 16: Performance of mTrack when tracking different numbers of mice.

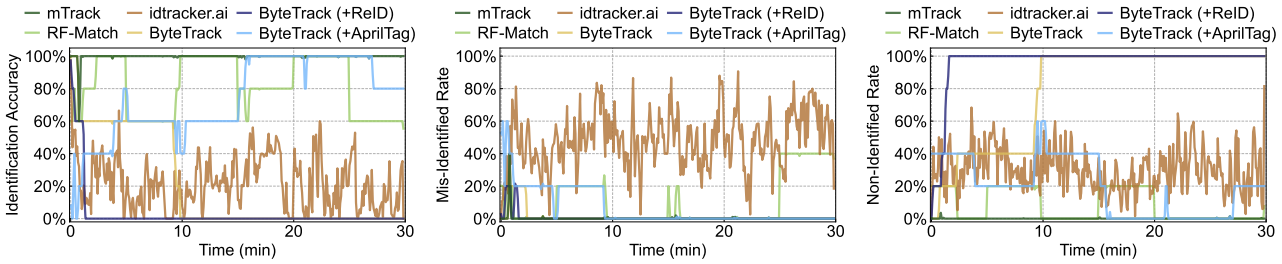

(a) Identification accuracy. (b) Mis-identified rate. (c) Non-identified rate.

Figure 17: Performance of mTrack when tracking five mice over 30 minutes.

8 Evaluation

8.1 Evaluation Setup

Mouse. We evaluate mTrack with C57BL/6J mice (a widely used lab strain) [70] in a biology lab. We use 80 mice from eight batches throughout the entire evaluation. Their ages are 6–8 weeks and weights are 20–23 g. In each comparison, we use mice from the same batch with similar ages and weights.

Groundtruth. To annotate the data, we first generate raw track annotations using ByteTrack [79], and then manually correct the raw annotations using the annotation tool CVAT [13]. Given the significant labeling effort required, we adopt a default experimental configuration of tracking 5 mice for 10 minutes unless otherwise specified. The full dataset in our evaluation includes approximately 5 hours of video.

Detector Model. The original YOLOv8 [32] does not directly support mouse detection. We collect 300 mouse images and split them into 200/50/50 for training/validation/testing to finetune it. The model converges in about 400 epochs, achieving 97% test accuracy. For the dark environment experiment, we finetune a low-light version using 30 training, 10 validation, and 10 testing infrared images under dark conditions, achieving 98% testing accuracy.

Metrics. We adopt the following identification metrics, aligned with previous research [69]:

- *Non-Identified Rate ($R_{non\text{-}id}$).* The percentage of mice per frame to which the tracker fails to assign any identity.
- *Mis-Identified Rate ($R_{mis\text{-}id}$).* The percentage of mice per frame that the system assigns the wrong identity to.
- *Identification Accuracy (A_{id}).* The percentage of mice per frame to which the system correctly assigns identities: $A_{\text{id}} = 1 - R_{\text{non-id}} - R_{\text{mis-id}}$.
- *Localization Precision.* The average localization error of the returned trajectories, determined by comparing them to the ground truth trajectories.

Baselines.

- *CV: ByteTrack [79].* A popular MOT baseline with strong robustness and performance in challenging real-world scenarios.
- *CV: ByteTrack [79] + ReID [80].* A modified version of ByteTrack with appearance-based ReID discussed in §2.1.
- *CV: ByteTrack [79] + AprilTag [50].* A modified version of ByteTrack integrating AprilTag to correct association errors. We use 1.5 cm × 1.5 cm tags from the 16h5 family for reliable detection at reduced dimensions.
- *CV: idtracker.ai [55].* A widely used open-source tool in biology that identifies individuals by appearance and uses the known number of tracked animals.
- *CV-RFID Fusion: RF-Match.* Our custom implementation of an RFID-visual tracklet matching algorithm via global optimization, extending the prior work TagView [22].

8.2 Overall Performance

Tracking Accuracy vs. Number. To evaluate the scalability of mTrack, we track 2 to 14 mice over 10 minutes. As shown in Fig. 16, mTrack achieves over 99% identification accuracy for 2 to 10 mice. Remaining <1% of frames remain unidentified, mostly consisting of short and inconsequential trajectory fragments caused by frequent occlusions when multiple mice gathered. These fragments are sporadically distributed throughout the experimental period. When tracking 12 and 14 mice, accuracy drops to 95.44% and 93.67%, respectively. This degradation reflects the limits of scalability: as population density increases, visual trajectories overlap more often,

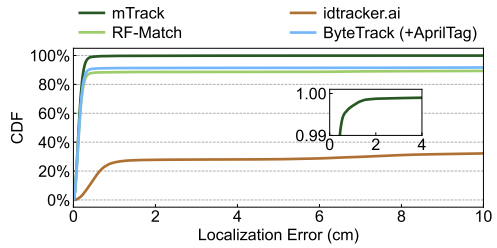

Figure 18: Localization precision.

causing higher association error frequency. Meanwhile, the matching algorithm converges more slowly due to the larger number of possible identity assignments, which increases the chance of failed identifications. Nevertheless, as shown in Tab. 1, mTrack still achieves a substantial scalability improvement over prior systems. RF-Match and ByteTrack with AprilTag form the second-best group of methods. RF-Match exhibits unstable and inadequate accuracy, ranging from 49.90% to 86.77% for more than four mice, primarily due to its sensitivity to inaccuracies — variance in match scores or imperfect constraint modeling can lead to significant errors. Additionally, while RF-Match can repair fragmentation errors by assigning identities to tracklets, it cannot correct the errors of ID switch. In contrast, mTrack incorporates a quality monitor that detects ID switches during tracking, thereby preventing error propagation. ByteTrack with AprilTag achieves inadequate accuracy, ranging from 77.04% to 86.50%. This is because the small size of the tags and motion blur during rapid movements lead to missed tag detections, resulting in failed identification. All the other CV-based methods exhibit poor identification accuracy below 73%. Two key takeaways are: (1) UHF RFID fusion effectively addresses identity association errors, and (2) the optimization from matching algorithm to tag scheduling allows mTrack to consistently maintain outstanding accuracy with a large number of mice.

Tracking Accuracy vs. Time. Long-term tracking is essential in biological research. To assess mTrack's reliability in long-term experiments, we track five mice for 30 minutes, recording average identification accuracy every five seconds. As shown in Fig. 17, mTrack maintains nearly 100% accuracy, quickly correcting any occasional errors. *In principle, mTrack can maintain high accuracy indefinitely due to the self-correcting capability.* In contrast, ByteTrack lost track of all five mice after 10 minutes, with 100% non-identified rate. Other baselines adopt appearance features or physical identifiers to correct errors, but they still suffer from high mis-identified and non-identified rates.

Localization Precision. Since ByteTrack fails to maintain correct identifications early on, its localization precision is no longer meaningful. Therefore, we only report the localization errors of mTrack, RF-Match, and idtracker.ai, as shown in Fig. 18. mTrack achieves a 99th-percentile localization error of 0.4 cm. By contrast, ByteTrack with AprilTag, RF-Match, and idtracker.ai exceed 10 cm error in 8%, 11%, and 68% of cases, respectively, large for scientific studies.

8.3 Performance Under Varied Conditions

We evaluate mTrack under different experiment conditions. As shown in Tab. 2, mTrack remains robust in most cases. The detailed results are discussed below:

Table 2: Performance under varied conditions.

	Conditions		
Mice Density	1.00 $m^2/5$	0.20 $m^2/5$	0.12 $m^2/5$
Accuracy	99.96%	99.60%	96.04%
# of Antennas	4	2	1
Accuracy	99.96%	99.82%	99.42%
Multipath	No	Static	Dynamic
Accuracy	99.96%	99.97%	99.95%
Light Condition	Daylight	Dark	
Accuracy	99.96%	99.82%	

Impact of Mice Density. We evaluate tracking at different densities by placing five mice in large (1 × 1 m, standard), medium (0.4 × 0.5 m, crowded), and small (0.3 × 0.4 m, highly crowded) cages. As density rises, tracking becomes harder. mTrack achieves 99.96% in the large cage and 99.60% in the medium cage, but drops to 96.04% in the small cage due to more frequent interactions. The high-density case is mainly a stress test; most real experiments are closer to the standard setup [27].

Impact of Antenna Number. mTrack uses four antennas for full coverage and no blind spots. Since some low-cost RFID readers support only one port, we test 4, 2, and 1 antennas. mTrack achieves 99.96%, 99.82%, and 99.42% identification accuracy, respectively. These results show that more antennas help, but even one antenna remains reliable for mouse tracking.

Impact of Multipath Interference. We evaluate mTrack under multipath in two scenarios: dynamic (a person walking nearby) and static (a 40 cm × 40 cm metal plate near the mouse cage). In both cases, mTrack stays above 99% accuracy, showing robustness to multipath interference.

Impact of Light Condition. Given that mice are nocturnal (*i.e.,* they prefer to be active in the dark), many behavior experiments are conducted in the darkness. Using an infrared camera, we confirm that mTrack maintains an accuracy of 99.82% in the dark environments, as expected since low-light conditions do not affect RFID-based identification.

8.4 Microbenchmarks

We validate the effectiveness of three key components of mTrack: RFID-vision trajectory matching, tracklet identity manager, and RFID reading scheduler.

Table 3: Performance of trajectory matching (§4).

# of Mice	2	4	6	8	10
Only Maximal	100.0%	100.0%	47.53%	60.52%	45.99%
+ Stable Condition	100.0%	100.0%	99.84%	75.00%	77.77%
+ Quality Monitor	100.0%	100.0%	99.95%	99.57%	99.23%

RFID-vision Trajectory Matching. mTrack's matching algorithm (§4) uses strict match conditions and a quality monitor for robust matching. Tab. 3 shows that the maximal condition alone achieves 100.0% accuracy for 2 or 4 mice. However, accuracy drops

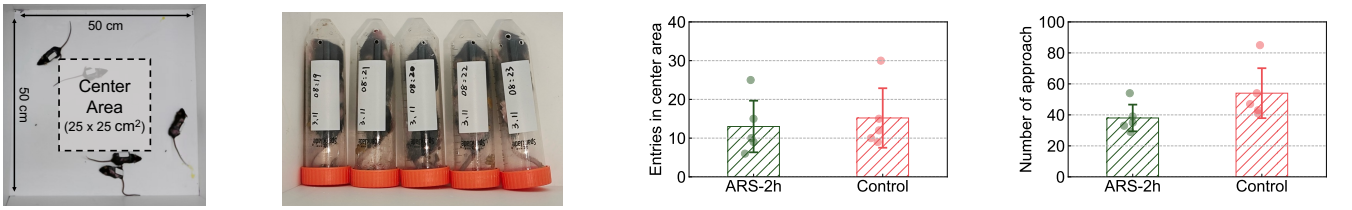

(a) Open field test. (b) Acute restraint stress. (c) Entries in center area. (d) Number of approaches.

Figure 19: Study of how acute stress-induced anxiety influences behaviors.

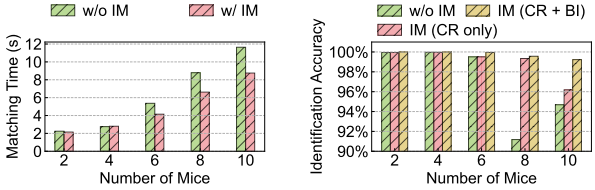

(a) Mean matching time. (b) Identification accuracy.

Figure 20: Performance of identity manager (§5).

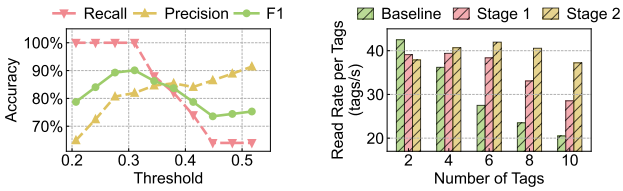

(a) Mobility estimation. (b) Reading rate gain.

Figure 21: Performance of reading scheduler (§6).

with more mice. This happens because when several mice move similarly, one visual trajectory can get high scores with multiple RFID tags. The stable condition improves this by only accepting unique high-score matches, yet accuracy for over eight mice remains below 80%. This persistent issue arises from ID switches within the visual tracker, which can corrupt matches and propagate errors to subsequent frames. Finally, integrating the quality monitor elevates the accuracy to over 99% for all cases.

Tracklet Identity Manager. mTrack introduces tracklet identity manager (IM) with two mechanisms: candidate reduction (CR) and backward identification (BI) to accelerate matching and correct historical errors. As shown in Fig. 20a, the manager reduces matching time by 1.2 to 2.9 seconds after each association error when tracking over 6 mice, achieving about 25% speed-up. End-to-end results (Fig. 20b) show that both mechanisms let mTrack scale while keeping over 99% accuracy. Identification accuracy without the identity manager is lowest (91%) for eight mice, not ten, likely due to random factors such as variations in interaction frequency.

RFID Reading Scheduler. The RFID reading scheduler operates in two stages: Stage 1 reads all unmatched tags and estimates their mobility classified as low-mobility (<5 cm/s) or high-mobility (≥5 cm/s). Stage 2 focuses on reading the high-mobility tags. First, we evaluate the accuracy of the mobility estimation with different thresholds C. Fig. 21a shows a maximal F1 score of 90%, with 100% recall and 82% precision, indicating reliable identification of high-mobility tags despite some low-mobility false positives. Next, we evaluate the read rate gain of each stage. We report the read rate of target tags in each stage and set the baseline as the read rate without scheduling. Fig. 21b shows that Stage 1 improves read rate by 3.2 ∼ 8.0 times/s for more than two tags by prioritizing unmatched tags instead of reading all tags. Stage 2 further improves it by 1.3 ∼ 8.7 times/s by focusing on high-mobility tags critical to matching convergence. For two tags, read rate drops slightly due to `select` overhead, suggesting the scheduler can be disabled for small mouse counts.

9 Field Study

We collaborated with biologists to conduct two field studies to demonstrate that mTrack can be seamlessly integrated into current behavioral analysis workflows and assist in biology research.

9.1 Long-term Tracking at Scale

We conduct a large-scale long-term experiment to validate mTrack's ability to keep high accuracy with multiple mice.

Experimental Setup. We conduct a two-hour experiment with ten mice in a 1 × 1 m open field under normal lighting conditions, the same setup as illustrated in Fig. 15. To evaluate mTrack's identification accuracy, five human experts perform a sample inspection of the tracking results. First, each expert assesses 24 shared frames (one every five minutes) for inter-expert consistency. Then, each expert independently evaluates 24 unique frames sampled every minute, totaling 120 frames.

Results. We assess inter-expert consistency using the Intraclass Correlation Coefficient (ICC) two-way random-effects model (ICC(2,n)). The results show high agreement among the five experts: ICC = 0.984 (95% CI [0.97, 0.99]), $F(23, 92) = 59.95$, $p < 0.001$. The final identification accuracy for the 24 frames independently evaluated by each expert is 98.7 ± 0.2%. This shows that mTrack reliably supports hours of high-accuracy tracking.

9.2 Acute Stress-Induced Anxiety

We conduct an experiment to investigate mouse behavior under acute stress-induced anxiety, demonstrating the potential of mTrack to enable social behavior analysis.

Experimental Setup. To model acute stress-induced anxiety, five mice were immobilized in modified plastic syringes with drilled holes for two hours [10] as the experimental group. Another five mice were allowed to move freely in the cages as the control group. A 10-minute tracking experiment was conducted separately for the two groups in a 50 cm × 50 cm open field, shown in Fig. 19a.

Results. Following the standard experimental methodology [10], we analyze the entries into the center area (25 cm × 25 cm). The control group exhibits more entries (15.0 ± 7.8) than the experimental group (12.6 ± 6.0), indicating that acute stress-induced anxiety reduces exploratory behavior. We also analyze the number of approaches between mice [23]. The control group shows more approaches (55.6 ± 16.4) than the experimental group (41.2 ± 9.2), suggesting greater social tendencies. The experimental results indicate that acute stress-induced anxiety leads to reduced exploratory and social tendencies in mice. Although not statistically significant due to limited replication, these results align with prior studies on anxious mouse behavior [10, 77], showing the potential of mTrack for behavioral and psychological research.

10 Discussion

Larger-scale Study. Current social behavior studies are often limited to two-mouse interactions due to tracking difficulty [72]. mTrack supports up to ten mice, enabling richer social-interaction and group-dynamics studies. Yet scaling to larger populations and spaces remains challenging because of software and hardware limits. With more mice (*e.g.,* 20), more frequent association errors challenge RFID identification speed. Also, the small tags have a limited read range of about 1.5 m. Future mTrack versions could use high-throughput, precise RFID localization [20, 39, 45] and multiple distributed readers to improve speed and coverage.

Tag Design and Attachment. In our setup, we use commercial UHF RFID tags measuring 1.5 cm × 2.5 cm, selected to fit the small body size of mice. Each tag weighs only 0.1 g, significantly lighter than typical laboratory animal tags [1, 56]. However, durability and potential impacts on animal welfare remain concerns. To address these issues, lightweight mounts—such as tail-attached fixtures [14]—could improve attachment robustness and lifespan. Customized flexible RFID tags [37, 81] may also improve comfort and reduce interference with natural behaviors.

Fine-grained Behavior Analysis. In our field study (§9.2), we measure behavioral metrics such as center-area entries and close approach frequency, both indicative of anxiety. Beyond these basics, patterns like sniffing, grooming, chasing, and attacking can offer deeper behavioral insights. Such fine-grained analysis clarifies behavior mechanisms [4] and provides precise metrics for evaluating pharmacological interventions [73]. Depending on experimental needs, advanced vision algorithms [46, 58] can be integrated into mTrack to support more detailed studies.

Extending to Other Applications. While mTrack targets mouse tracking, it can be extended to other animals, such as rats or pigeons. In addition, RFID-vision integration can ground semantic information — linking abstract concepts to real-world entities in embodied AI. By tagging objects with RFID and associating metadata with visual detections, mTrack enables agents to build actionable world models and adapt to new objects and environments.

11 Related Work

Visual Tracking. Multi-object tracking is a fundamental research area in computer vision [6, 74, 79]. Various tracking algorithms have been developed, including SORT [6], DeepSORT [74], ByteTrack [79], and BoT-SORT [2], all of which have demonstrated strong performance on human- and vehicle-centric benchmarks [47, 61]. In biological research, visual tracking tools such as idtracker.ai [55], DeepLabCut [46], AlphaTracker [11], and Trex [64] are widely used. These methods rely on motion continuity and appearance similarity for tracking and identification. In mouse tracking, however, their performance drops sharply, especially for long-term ID accuracy, because mice look alike and move erratically. mTrack mitigates these challenges by incorporating a physical identifier—UHF RFID—for robust long-term identification.

RFID Tracking. UHF RFID localization and tracking have been widely studied, leveraging backscattered signals to estimate tag locations. Prior work improves localization with dense reference tags [65], multiple antennas [66], inverse synthetic aperture radar [75], tag arrays [8, 68], and wideband methods [20, 39, 45]. However, none of these systems can achieve reliable centimeter-level localization within milliseconds due to the inherent bandwidth and communication limitations of RFID. As an alternative, mTrack integrates a visual tracker for precise detection and localization while leveraging UHF RFID for tracklet identification, ensuring robust and accurate mouse tracking.

RFID-Vision Hybrid Tracking. UHF RFID has proven effective for object identification when combined with visual data in applications like human-object interaction [36, 43] and smart retail [67]. TagVision [21], TagView [22], and TagFocus [76] use global optimization-based matching [35] but are sensitive to inaccuracies — variance in match scores or imperfect constraint modeling can lead to significant errors. RF-Focus [67] and ID-Match [36] match phase sequences and visual data at fixed intervals, but ignore matching confidence, causing instability. Additionally, these systems typically assume constrained motion patterns, where visual trackers seldom make association errors. In contrast, mouse tracking involves frequent identity association errors due to complex, unpredictable movements. mTrack tackles this with an online matching framework with quality monitoring to maintain high accuracy over time.

Mouse Tracking. ID errors remain a persistent challenge in mouse tracking, prompting the use of conventional tags such as QR codes [14] and High-frequency (HF, 134.2 kHz) RFID [19, 52, 69]. QR codes, however, are unsuitable for long-term tracking, as motion blur, food residues, or hair often obscure them, degrading recognition accuracy [3]. HF RFID, common in laboratory management [71], enables short-range (<10 cm) identification and coarse localization. Yet it has two drawbacks: no anti-collision protocol [71], which causes failures when multiple mice are nearby, and poor scalability from dense antenna deployment (e.g., 39 per m^2 [69]) and slow reads (20–100 ms per tag). mTrack instead adopts UHF RFID for longer range and higher rate. mTrack is the first UHF RFID-based mouse tracking system, enabling scalable and efficient mouse tracking.

12 Conclusion

In this paper, we demonstrate that visual trackers suffer persistent identity association errors in laboratory mouse tracking due to similar appearance and frequent occlusions. To address this challenge, we introduce mTrack, the first UHF RFID-vision hybrid tracking system. It combines robust UHF RFID identification with precise

visual localization, enabling long-term, self-correcting, and high-accuracy mouse tracking. We believe mTrack provides a reliable and practical multi-mouse tracking solution for biologists and can support new discoveries in neurological mechanisms and potential therapeutic interventions.

Acknowledgments

This work is supported by National Key R&D Program of China (Grant No.2023YFF0725004), National Natural Science Foundation of China (Grant No. U25B2040, 62502012 and 62272010), and the Postdoctoral Fellowship Program and China Postdoctoral Science Foundation (Grant No. GZC20251070). Chenren Xu is the corresponding author.

References

[1] AgnThos. 2025. RapID Tags. https://agnthos.se/rapid-tags/1018-rapid-tags.html.
[2] Nir Aharon, Roy Orfaig, and Ben-Zion Bobrovsky. 2022. Bot-sort: Robust associations multi-pedestrian tracking. *arXiv:2206.14651* (2022).
[3] Gustavo Alarcón-Nieto, Jacob M Graving, James A Klarevas-Irby, Adriana A Maldonado-Chaparro, Inge Mueller, and Damien R Farine. 2018. An automated barcode tracking system for behavioural studies in birds. *Methods in Ecology and Evolution* 9, 6 (2018).
[4] Diego Aldarondo, Josh Merel, Jesse D Marshall, Leonard Hasenclever, Ugne Klibaite, Amanda Gellis, Yuval Tassa, Greg Wayne, Matthew Botvinick, and Bence P Ölveczky. 2024. A virtual rodent predicts the structure of neural activity across behaviours. *Nature* 632, 8025 (2024).
[5] Alien. 2025. Alien Readers. https://www.alientechnology.com/products/readers/.
[6] Alex Bewley, Zongyuan Ge, Lionel Ott, Fabio Ramos, and Ben Upcroft. 2016. Simple online and realtime tracking. In *IEEE ICIP*.
[7] G. Bradski. 2000. The OpenCV Library. *Dr. Dobb's Journal of Software Tools* (2000).
[8] Yanling Bu, Lei Xie, Yinyin Gong, Chuyu Wang, Lei Yang, Jia Liu, and Sanglu Lu. 2018. RF-Dial: An RFID-based 2D human-computer interaction via tag array. In *IEEE INFOCOM*.
[9] Alberto Caprara, Paolo Toth, and Matteo Fischetti. 2000. Algorithms for the set covering problem. *Annals of Operations Research* 98, 1 (2000).
[10] Danyang Chen, Qianqian Lou, Xiang-Jie Song, Fang Kang, An Liu, Changjian Zheng, Yanhua Li, Di Wang, Sen Qun, Zhi Zhang, et al. 2024. Microglia govern the extinction of acute stress-induced anxiety-like behaviors in male mice. *Nature Communications* 15, 1 (2024).
[11] Zexin Chen, Ruihan Zhang, Hao-Shu Fang, Yu E Zhang, Aneesh Bal, Haowen Zhou, Rachel R Rock, Nancy Padilla-Coreano, Laurel R Keyes, Haoyi Zhu, et al. 2023. AlphaTracker: a multi-animal tracking and behavioral analysis tool. *Frontiers in Behavioral Neuroscience* 17 (2023).
[12] Amy E Clipperton-Allen and Damon T Page. 2022. Social behavior testing in mice: Social interest, recognition, and aggression. In *Psychiatric Vulnerability, Mood, and Anxiety Disorders: Tests and Models in Mice and Rats*. Springer.
[13] CVAT.ai Corporation. 2023. *Computer Vision Annotation Tool (CVAT)*. doi:10.5281/zenodo.8070041
[14] Vincent Coulombe, Arturo Marroquin Rivera, Sadegh Monfared, David-Alexandre Roussel, Quentin Leboulleux, Modesto R Peralta III, Benoit Gosselin, and Benoit Labonté. 2025. The Tailtag: A multi-mouse tracking system to measure social dynamics in complex environments. *Neuropsychopharmacology* (2025), 1–10.
[15] James D Crall, Nick Gravish, Andrew M Mountcastle, and Stacey A Combes. 2015. BEEtag: a low-cost, image-based tracking system for the study of animal behavior and locomotion. *PloS one* 10, 9 (2015).
[16] Fabrice De Chaumont, Elodie Ey, Nicolas Torquet, Thibault Lagache, Stéphane Dallongeville, Albane Imbert, Thierry Legou, Anne-Marie Le Sourd, Philippe Faure, Thomas Bourgeron, et al. 2019. Real-time analysis of the behaviour of groups of mice via a depth-sensing camera and machine learning. *Nature biomedical engineering* 3, 11 (2019).
[17] Daniel D Deavours. 2010. Improving the near-metal performance of UHF RFID tags. In *IEEE RFID*.
[18] Victor H Denenberg. 1969. Open-field behavior in the rat: What does it mean? *Annals of the New York Academy of Sciences* 159, 3 (1969), 852–859.
[19] Ashesh K Dhawale, Rajesh Poddar, Steffen BE Wolff, Valentin A Normand, Evi Kopelowitz, and Bence P Ölveczky. 2017. Automated long-term recording and analysis of neural activity in behaving animals. *Elife* 6 (2017).
[20] Laura Dodds, Isaac Perper, Aline Eid, and Fadel Adib. 2023. A handheld fine-grained rfid localization system with complex-controlled polarization. In *ACM MobiCom*.
[21] Chunhui Duan, Xing Rao, Lei Yang, and Yunhao Liu. 2017. Fusing RFID and computer vision for fine-grained object tracking. In *IEEE INFOCOM*.
[22] Chunhui Duan, Wenlei Shi, Fan Dang, and Xuan Ding. 2020. Enabling RFID-based tracking for multi-objects with visual aids: A calibration-free solution. In *IEEE INFOCOM*.
[23] Nozomi Endo, Waka Ujita, Masaya Fujiwara, Hideaki Miyauchi, Hiroyuki Mishima, Yusuke Makino, Lisa Hashimoto, Hiroshi Oyama, Manabu Makinodan, Mayumi Nishi, et al. 2018. Multiple animal positioning system shows that socially-reared mice influence the social proximity of isolation-reared cagemates. *Communications biology* 1, 1 (2018).
[24] EPCglobal. 2024. EPC UHF Gen2 Air Interface Protocol. https://www.gs1.org/standards/rfid/uhf-air-interface-protocol.
[25] Theodore Garland Jr, Todd T Gleeson, Benjamin A Aronovitz, Christopher S Richardson, and Michael R Dorm. 1995. Maximal sprint speeds and muscle fiber composition of wild and laboratory house mice. *Physiology & behavior* 58, 5 (1995).
[26] GS1. 2024. Low Level Reader Protocol. https://www.gs1.org/standards/epc-rfid/epc-rfid-llrp/2-0.
[27] Calvin Hall and Egerton L Ballachey. 1932. A study of the rat's behavior in a field. A contribution to method in comparative psychology. *University of California Publications in Psychology* (1932).
[28] Impinj. 2023. Application Note: Low-Level User Data Support. https://support.impinj.com/hc/en-us/articles/202755318-Application-Note-Low-Level-User-Data-Support.
[29] Impinj. 2025. Impinj R700 Series RAIN RFID Readers. https://www.impinj.com/products/readers/impinj-r700.
[30] Impinj. 2025. Impinj Speedway RAIN RFID Readers. https://www.impinj.com/products/readers/impinj-speedway.
[31] Impinj. 2025. Octane SDK. https://support.impinj.com/hc/en-us/articles/202755268-Octane-SDK.
[32] Glenn Jocher, Jing Qiu, and Ayush Chaurasia. 2023. *Ultralytics YOLO*. https://github.com/ultralytics/ultralytics
[33] Oksana Kaidanovich-Beilin, Tatiana Lipina, Igor Vukobradovic, John Roder, and James R Woodgett. 2011. Assessment of social interaction behaviors. *Journal of visualized experiments* 48 (2011).
[34] Navjot Kaur, Diana Segura Velandia, William Whittow, David Barwick, Ehidiamen Iredia, Neil Parker, Neil Porter, Paul P Conway, and Andrew A West. 2015. Design and performance of a flexible metal mountable UHF RFID tag. In *IEEE ECTC*.
[35] Harold W Kuhn. 1955. The Hungarian method for the assignment problem. *Naval research logistics quarterly* 2, 1-2 (1955).
[36] Hanchuan Li, Peijin Zhang, Samer Al Moubayed, Shwetak N Patel, and Alanson P Sample. 2016. Id-match: A hybrid computer vision and rfid system for recognizing individuals in groups. In *ACM CHI*.
[37] Liyao Li, Bozhao Shang, Yun Wu, Jie Xiong, Xiaojiang Chen, and Yaxiong Xie. 2024. Cyclops: A Nanomaterial-based, Battery-Free Intraocular Pressure (IOP) Monitoring System inside Contact Lens. In *USENIX NSDI*.
[38] Yuan Li, Chang Huang, and Ram Nevatia. 2009. Learning to associate: Hybridboosted multi-target tracker for crowded scene. In *IEEE CVPR*.
[39] Bo Liang, Purui Wang, Renjie Zhao, Heyu Guo, Pengyu Zhang, Junchen Guo, Shunmin Zhu, Hongqiang Harry Liu, Xinyu Zhang, and Chenren Xu. 2023. RFChord: Towards deployable RFID localization system for logistic networks. In *USENIX NSDI*.
[40] Qiongzheng Lin, Lei Yang, Huanyu Jia, Chunhui Duan, and Yunhao Liu. 2017. Revisiting reading rate with mobility: Rate-adaptive reading in COTS RFID systems. In *CoNEXT*.
[41] Bingbin Liu, Yuxuan Qian, and Jianxin Wang. 2023. EDDSN-MRT: multiple rodent tracking based on ear detection and dual siamese network for rodent social behavior analysis. *BMC neuroscience* 24, 1 (2023).
[42] Jia Liu, Xingyu Chen, Xiulong Liu, Xiaocong Zhang, Xia Wang, and Lijun Chen. 2019. On improving write throughput in commodity RFID systems. In *IEEE INFOCOM*.
[43] Xiulong Liu, Dongdong Liu, Jiuwu Zhang, Tao Gu, and Keqiu Li. 2021. RFID and camera fusion for recognition of human-object interactions. In *ACM MobiCom*.
[44] Jonathon Luiten, Aljosa Osep, Patrick Dendorfer, Philip Torr, Andreas Geiger, Laura Leal-Taixé, and Bastian Leibe. 2021. Hota: A higher order metric for evaluating multi-object tracking. *IJCV* 129 (2021).
[45] Yunfei Ma, Nicholas Selby, and Fadel Adib. 2017. Minding the billions: Ultra-wideband localization for deployed RFID tags. In *ACM MobiCom*.
[46] Alexander Mathis, Pranav Mamidanna, Kevin M Cury, Taiga Abe, Venkatesh N Murthy, Mackenzie Weygandt Mathis, and Matthias Bethge. 2018. DeepLabCut: markerless pose estimation of user-defined body parts with deep learning. *Nature neuroscience* 21, 9 (2018).
[47] Anton Milan, Laura Leal-Taixé, Ian Reid, Stefan Roth, and Konrad Schindler. 2016. MOT16: A benchmark for multi-object tracking. *arXiv:1603.00831* (2016).
[48] NXP. 2024. UCODE 9xe: UCODE 9 with more EPC Memory. https://www.nxp.com/products/rfid-nfc/ucode-rain-rfid-uhf/ucode-9xe-ucode-9-with-more-epc-memory:UCODE-9xe.

[49] Shay Ohayon, Ofer Avni, Adam L Taylor, Pietro Perona, and SE Roian Egnor. 2013. Automated multi-day tracking of marked mice for the analysis of social behaviour. *Journal of neuroscience methods* 219, 1 (2013).

[50] Edwin Olson. 2011. AprilTag: A robust and flexible visual fiducial system. In *IEEE ICRA*.

[51] Veronica Panadeiro, Alvaro Rodriguez, Jason Henry, Donald Wlodkowic, and Magnus Andersson. 2021. A review of 28 free animal-tracking software applications: current features and limitations. *Lab animal* 50, 9 (2021).

[52] Tatiana Peleh, Xuesheng Bai, Martien JH Kas, and Bastian Hengerer. 2019. RFID-supported video tracking for automated analysis of social behaviour in groups of mice. *Journal of Neuroscience Methods* 325 (2019).

[53] Ergys Ristani, Francesco Solera, Roger Zou, Rita Cucchiara, and Carlo Tomasi. 2016. Performance measures and a data set for multi-target, multi-camera tracking. In *ECCV*.

[54] Alvaro Rodriguez, Hanqing Zhang, Jonatan Klaminder, Tomas Brodin, Patrik L Andersson, and Magnus Andersson. 2018. ToxTrac: a fast and robust software for tracking organisms. *Methods in Ecology and Evolution* 9, 3 (2018).

[55] Francisco Romero-Ferrero, Mattia G Bergomi, Robert C Hinz, Francisco JH Heras, and Gonzalo G De Polavieja. 2019. Idtracker. ai: tracking all individuals in small or large collectives of unmarked animals. *Nature methods* 16, 2 (2019).

[56] Johnny V Roughan and Tatum Sevenoaks. 2019. Welfare and scientific considerations of tattooing and ear tagging for mouse identification. *Journal of the American Association for Laboratory Animal Science* 58, 2 (2019).

[57] Kristina Rydell-Törmänen and Jill R Johnson. 2019. The applicability of mouse models to the study of human disease. *Mouse cell culture: methods and protocols* (2019).

[58] Cristina Segalin, Jalani Williams, Tomomi Karigo, May Hui, Moriel Zelikowsky, Jennifer J Sun, Pietro Perona, David J Anderson, and Ann Kennedy. 2021. The Mouse Action Recognition System (MARS) software pipeline for automated analysis of social behaviors in mice. *Elife* 10 (2021).

[59] Longfei Shangguan and Kyle Jamieson. 2016. The design and implementation of a mobile RFID tag sorting robot. In *ACM MobiSys*.

[60] Justin C Strickland and Mark A Smith. 2015. Animal models of social contact and drug self-administration. *Pharmacology Biochemistry and Behavior* 136 (2015).

[61] Peize Sun, Jinkun Cao, Yi Jiang, Zehuan Yuan, Song Bai, Kris Kitani, and Ping Luo. 2022. Dancetrack: Multi-object tracking in uniform appearance and diverse motion. In *IEEE/CVF CVPR*.

[62] Yu-Ting Tseng, Binghao Zhao, Hui Ding, Lisha Liang, Bernhard Schaefke, and Liping Wang. 2023. Systematic evaluation of a predator stress model of depression in mice using a hierarchical 3D-motion learning framework. *Translational Psychiatry* 13, 1 (2023).

[63] Ultralytics. 2025. Ultralytics. https://www.ultralytics.com/.

[64] Tristan Walter and Iain D Couzin. 2021. TRex, a fast multi-animal tracking system with markerless identification, and 2D estimation of posture and visual fields. *Elife* 10 (2021).

[65] Jue Wang and Dina Katabi. 2013. Dude, where's my card? RFID positioning that works with multipath and non-line of sight. In *ACM SIGCOMM*.

[66] Jue Wang, Deepak Vasisht, and Dina Katabi. 2014. RF-IDraw: Virtual touch screen in the air using RF signals. In *ACM SIGCOMM*.

[67] Zhongqin Wang, Min Xu, Ning Ye, Ruchuan Wang, and Haiping Huang. 2019. RF-Focus: Computer vision-assisted region-of-interest RFID tag recognition and localization in multipath-prevalent environments. *ACM IMWUT* 3, 1 (2019).

[68] Teng Wei and Xinyu Zhang. 2016. Gyro in the air: tracking 3d orientation of batteryless internet-of-things. In *ACM MobiCom*.

[69] Aharon Weissbrod, Alexander Shapiro, Genadiy Vasserman, Liat Edry, Molly Dayan, Assif Yitzhaky, Libi Hertzberg, Ofer Feinerman, and Tali Kimchi. 2013. Automated long-term tracking and social behavioural phenotyping of animal colonies within a semi-natural environment. *Nature communications* 4, 1 (2013).

[70] Wikipedia. 2025. C57BL/6 Mouse. https://en.wikipedia.org/wiki/C57BL/6.

[71] Wikipedia. 2025. ISO 11784 and ISO 11785. https://en.wikipedia.org/wiki/ISO_11784_and_ISO_11785.

[72] Cait M Williamson, Becca Franks, and James P Curley. 2016. Mouse social network dynamics and community structure are associated with plasticity-related brain gene expression. *Frontiers in Behavioral Neuroscience* 10 (2016), 152.

[73] Alexander B Wiltschko, Tatsuya Tsukahara, Ayman Zeine, Rockwell Anyoha, Winthrop F Gillis, Jeffrey E Markowitz, Ralph E Peterson, Jesse Katon, Matthew J Johnson, and Sandeep Robert Datta. 2020. Revealing the structure of pharmacobehavioral space through motion sequencing. *Nature neuroscience* 23, 11 (2020).

[74] Nicolai Wojke, Alex Bewley, and Dietrich Paulus. 2017. Simple online and realtime tracking with a deep association metric. In *IEEE ICIP*.

[75] Lei Yang, Yekui Chen, Xiang-Yang Li, Chaowei Xiao, Mo Li, and Yunhao Liu. 2014. Tagoram: Real-time tracking of mobile RFID tags to high precision using COTS devices. In *ACM MobiCom*.

[76] Junjie Yin, Zheng Yang, Sicong Liao, Chunhui Duan, Xuan Ding, and Li Zhang. 2023. TagFocus: Towards fine-grained multi-object identification in RFID-based systems with visual aids. *ACM Transactions on Sensor Networks* 19, 1 (2023).

[77] Xiao-Dan Yu, Yi Zhu, Qi-Xin Sun, Fei Deng, Jinxia Wan, Di Zheng, Wankun Gong, Shi-Ze Xie, Chen-Jie Shen, Jia-Yu Fu, et al. 2022. Distinct serotonergic pathways to the amygdala underlie separate behavioral features of anxiety. *Nature neuroscience* 25, 12 (2022).

[78] Libo Zhang, Junyuan Gao, Zhen Xiao, and Heng Fan. 2023. AnimalTrack: A benchmark for multi-animal tracking in the wild. *IJCV* 131, 2 (2023).

[79] Yifu Zhang, Peize Sun, Yi Jiang, Dongdong Yu, Fucheng Weng, Zehuan Yuan, Ping Luo, Wenyu Liu, and Xinggang Wang. 2022. Bytetrack: Multi-object tracking by associating every detection box. In *ECCV*.

[80] Kaiyang Zhou, Yongxin Yang, Andrea Cavallaro, and Tao Xiang. 2019. Omni-scale feature learning for person re-identification. In *IEEE/CVF ICCV*.

[81] Haochen Zou, Zhibo Zhou, Mengyao Huang, Wenhao Li, Bowen Yang, Xiao Zhao, Ting Li, Lijie Xu, Ting Wang, and Lianhui Wang. 2025. NFC/RFID-enabled wearables and implants for biomedical applications. *Microsystems & Nanoengineering* 11, 1 (2025), 191.